Journal of Nuclear Medicine, published on December 7, 2017 as doi:10.2967/jnumed.117.201525

Radiolabeled (4-Fluoro-3-iodobenzyl)guanidine improves imaging and targeted radionuclide therapy of norepinephrine transporter-expressing tumors

Aiko Yamaguchi[1], Hirofumi Hanaoka[1], Tetsuya Higuchi[2], Yoshito Tsushima[2]

[1]Department of Bioimaging Information Analysis and [2]Department of Diagnostic Radiology and Nuclear Medicine, Gunma University Graduate School of Medicine, Maebashi, Japan

Corresponding author: Hirofumi Hanaoka, 3-39-22 Showa, Maebashi, Gunma 371-8511 Japan. Tel.: +81-27-220-8403; Fax: +81-27-220-8409; E-mail: hanaokah@gunma-u.ac.jp

First author: Aiko Yamaguchi, an assistant professor, 3-39-22 Showa, Maebashi, Gunma 371-8511 Japan. Tel.: +81-27-220-8403; Fax: +81-27-220-8409; E-mail: ayamaguchi@gunma-u.ac.jp

Word count: 4,974 (abstract: 219)

Financial support: This work is supported by JSPS KAKENHI Grant 26860981 for A. Yamaguchi.

Running title: Synthesis and evaluation of FIBG

ABSTRACT

$^{18}F/^{131}I$-labeled (4-Fluoro-3-iodobenzyl)guanidine (FIBG) have been a promising yet unattainable derivative of radioiodine-labeled meta-iodobenzylguanidine (MIBG), because of the complex radiofluorination method. Here, we proposed a 2-step radiosynthetic method for ^{18}F-FIBG, and evaluated the diagnostic and therapeutic potential of ^{18}F-FIBG and ^{131}I-FIBG in a pheochromocytoma model (PC-12). **Methods:** ^{18}F-FIBG was prepared from a (mesityl)(aryl)iodonium salt precursor in the presence of a copper-catalyst. Biodistribution studies, PET imaging, and therapeutic study were performed on the PC-12 xenograft mice with either ^{18}F- or ^{131}I-FIBG. The association between the therapeutic effect and the tumor uptake of pre-therapy ^{18}F-FIBG-PET was also evaluated. **Results:** The copper-mediated radiofluorination method readily yielded ^{18}F-FIBG, as well as its regioisomer, ^{18}F-IFBG. The isolated ^{18}F-FIBG showed higher accumulation in the PC-12 xenograft tumor than in any other organ. The high tumor uptake of ^{18}F-FIBG allowed clear tumor visualization in the PET image as early as 1 h after injection, with an excellent tumor-to-background ratio. A biodistribution study with ^{131}I-FIBG revealed its higher and prolonged retention in the tumor in comparison with MIBG. As a result, a therapeutic dose of ^{131}I-FIBG delayed tumor growth significantly more than ^{131}I-MIBG. The tumor uptake of ^{18}F-FIBG was proportional to the therapeutic effect of ^{131}I-FIBG. **Conclusion:** These results suggest the potential usefulness of FIBG as a diagnostic and therapeutic agent for the management of NET-expressing tumors.

Key Words: pheochromocytoma, neuroblastoma, MIBG analog, PET, targeted radionuclide therapy

INTRODUCTION

Radioiodine-labeled MIBG plays roles in the diagnosis and treatment of neuroblastomas and malignant pheochromocytomas (*1-3*) . ^{123}I-MIBG is preferred for diagnostic imaging, whereas ^{131}I-MIBG therapy has resulted in a noticeable response rate: most patients with malignant pheochromocytomas achieved disease stabilization, and approximately 30% of relapsed or refractory patients with neuroblastomas achieved a complete or partial response to therapy. Despite the abovementioned clinical usefulness, both radioiodine-labeled MIBGs have their limitations (*1,2,4*) and thus, attempts have been made to develop alternative MIBG derivatives (*5-8*).

Among the MIBG derivatives developed thus far, a promising pair of candidates is the combination of ^{18}F- and ^{131}I-labeled FIBG (**Fig. 1A**) (*8*). While both MIBGs and FIBGs can offer integrated diagnosis and therapy by the structurally identical agents, FIBGs may provide additional value as it allows radiolabeling with ^{18}F, the most frequently used positron emitter isotope. The diagnostic superiority of PET probe over single-photon probe for image-guided therapy is exemplified by the success of radiolabeled peptides targeting somatostatin receptors (*9*). The MIBG derivatives evaluated in this study, ^{18}F/^{131}I-FIBG, showed basic properties comparable to or superior to MIBG in cellular and normal mice studies (*10,11*). However, likely due to the complex radiosynthesis of ^{18}F-FIBG (*8*), further properties, such as tumor uptake and the therapeutic effectiveness of ^{131}I-FIBG, remain unknown.

Recently, owing to the developments in the transition-metal-mediated radiofluorination methods

of arenes, simple preparations of various ^{18}F-fluoroarenes have become possible, including probes that were previously difficult to develop (*12*). Given the applicability of these techniques to the radiosynthesis of another MIBG analog, meta-^{18}F-fluorobenzylguanidine (MFBG) (*13-15*), we hypothesized that the synthesis of ^{18}F-FIBG could be simplified by adapting one of these methods.

In this study, we developed a 2-step ^{18}F-FIBG preparation method using the Cu-mediated fluorination of mesityl(aryl)iodonium salt technique developed by Sanford and Scott (*16*). The usefulness of ^{18}F-FIBG for the detection and ^{131}I-FIBG for the treatment of NET-expressing tumors was evaluated using a pheochromocytoma xenograft mice.

MATERIALS AND METHODS

Unless otherwise stated, reagents and solvents were commercially available and used without further purification. Reagents were purchased from Sigma-Aldrich, TCI, or Wako. No-carrier-added radioiodinated MIBG derivatives were prepared as described (*17*).

Synthesis of Iodonium Salt Precursors (6a, b)

The mesityl-iodonium salt precursors are prepared according to the literatures (*15,16*) with slight modifications (**Fig. 1B**). Cold fluorination reaction was performed as previously described (**Supplemental Fig. 1A**) (*16*).

Synthesis of ^{18}F-FIBG and ^{18}F-IFBG (8a, b)

^{18}F-Fluoride was produced via the ^{18}O(p,n)^{18}F nuclear reaction using a cyclotron at Gunma University Hospital. The ^{18}F-labeling of the intermediate compound (**7a, b**) was performed as previously described (*16*) with subtle modifications (**Fig. 1C**). A 2 mL of water and a grain of Chelex 100 Chelating Resin (Bio-Rad) was then added to the reaction vial to trap the Cu-ion. The mixture was diluted with additional 10 mL of water and subjected onto a C18 Sep-Pak via a filtration unit. Unreacted ^{18}F was washed with additional 10 mL of water and the column was dried with N_2. The mixture **7a** and **b** were eluted with 1.5 mL of CH_3CN into a glass tube. The elution was evaporated with a stream of N_2 at 60°C,

then the deprotection reaction was performed with TFA at 75°C. After 15 min, the solvent was evaporated with a stream of N_2. The resulting regioisomer mixture of [^{18}F]FIBG and [^{18}F]IFBG (**8a, b**) was diluted with approximately 1 mL of 25/75 MeOH/H_2O, and the regioisomers were separated using semi-preparative high-performance liquid chromatography (HPLC). The radiochemical yield (RCY) of the intermediate compound (**7a, b**) was determined by dividing the integrated area under the objective compound spot by the total integrated area of the thin-layer chromatography plate (**Supplemental Fig. 2**).

Cellular Studies for MIBG Derivatives

The rat pheochromocytoma cell line PC-12 was obtained from American Type Culture Collection. The cellular uptake studies for ^{18}F-FIBG and ^{18}F-IFBG were performed as described (*10*). The cellular uptake and release profiles of ^{131}I-MIBG and ^{125}I-FIBG in a 3D cell culture model, and cellular therapeutic study for ^{131}I-FIBG and ^{131}I-MIBG were performed as previously described (*11*) with subtle modifications. For 3D culture model, the PC-12 cells were seeded into 96-well Nunclon Sphera microplates (Thermo Fisher Scientific, 1.0×10^5 cells/well) 24 hours before experiments.

Preparation of PC-12-Bearing Mice

All experimental protocols were approved by the Laboratory Animal Care and Use Committee of Gunma University. Five- to seven-week-old female BALB/c-nu/nu mice (Japan SLC) were inoculated

with PC-12 cells (5×10^6 cells/mouse) in the flank. Approximately 3 weeks after inoculation, the experiments described below were performed.

Tissue Distribution in Mice

Two studies were conducted in PC-12-bearing mice. First, a biodistribution study was performed in a paired-label format by co-injecting the mice with 50 kBq of ^{18}F-labeled and 5 kBq of ^{125}I-labeled MIBG derivatives (^{18}F-FIBG + ^{125}I-FIBG, ^{18}F-IFBG + ^{125}I-IFBG, or the regioisomer mixture + ^{125}I-MIBG, 4–5 mice per group) at 1 h post-injection. Next, a biodistribution study was also performed in a paired-label format by co-injecting the mice with 5 kBq each of ^{125}I-MIBG and ^{131}I-FIBG at 1, 3, 6, 24, and 48 h (4–5 mice per group), as well as 5 days post-injection (3 mice per group). In both studies, the mice were humanely killed by decapitation. The tissues of interest were isolated and weighed. A gamma counter (ARC7001; Hitachi Aloka Medical) was used to determine ^{18}F, ^{125}I, or ^{131}I activity. Another biodistribution study was performed in normal mice with the injection of 50 kBq each of ^{125}I-FIBG or ^{125}I-MIBG, and the absorbed radiation dose in humans were estimated by using OLINDA/EXM version 1.1 program (Vanderbilt University).

PET Imaging and Image Analysis

The PC-12-bearing mice were intravenously administered 1–2 MBq of ^{18}F-FIBG, ^{18}F-IFBG, or

the regioisomer mixture**.** The mice were anesthetized using isoflurane inhalation, and PET scans were performed 1 h and 2 h after administration of the MIBG derivative using a small animal PET scanner (Inveon; Siemens) with 10 min emission scanning. For ^{18}F-FDG-PET imaging, the PC-12-bearing mice were intravenously administered 5 MBq of ^{18}F-FDG after a 12 h fast, on the next day of ^{18}F-FIBG-PET imaging. PET imaging was performed as described above. Semi-quantitative analysis was performed for each identified tumor using AMIDE software (Stanford University). Volumes of interest were drawn manually to trace the contours of the tumor without correcting for partial volume effects. The background region of interest was placed in the muscles surrounding the shoulder. The mean tumor uptake was divided by the mean background uptake to calculate the tumor-to-background ratio. The SUV_{max} was determined by using Inveon Research Workplace workstation (Siemens).

Therapeutic Study In Vivo

When the tumors were fully established (0.16 ± 0.08 cm^3), the animals were randomly assigned to groups. There was no significant difference of the average tumor size between the groups. The mice were intravenously administered ^{131}I-MIBG (10 MBq) or ^{131}I-FIBG (1, 3, 5, or 10 MBq). Saline-injected mice were used as controls. At least 5 mice were allotted to each group, with the exception of the ^{131}I-FIBG 1 MBq group, which consisted of only 3 mice. The weight and tumor diameters of the mice were measured regularly. The tumor volumes were determined using the following formula: (length) × (width)^2

× 0.5. Each tumor volume was divided by the initial tumor volume to determine the relative tumor volumes. To evaluate the relationship between ^{18}F-FIBG uptake and the therapeutic effect of ^{131}I-FIBG, 5 MBq each of ^{131}I-FIBG was injected to the animals on the next day of ^{18}F-FDG-PET imaging (two days after the ^{18}F-FIBG-PET imaging), and animals were monitored as described above.

Statistical analyses

GraphPad Prism was used for the statistical analyses. Data are presented as mean ± SD. Statistical significance are reported based on the Student *t* test (a two-sample test or a paired test) or analysis of variance with Tukey's post-hoc test where appropriate. Simple correlation between variables was analyzed using a Pearson's correlation coefficient. Values of $P < 0.05$ were considered statistically significant.

RESULTS

Synthesis of Iodonium Salt Precursors (6a, b)

The direct one-pot oxidation/iodine arylation of **4** with mesytil-BF_3K yielded a mixture of *p*- and *m*- substituted unsymmetrical diaryliodonium triflates (**5a, b**), which were difficult to separate by silica gel-chromatography. As attempts to produce isomerically pure **5a** failed, a regioisomer mixture was used in the following experiments. An anion metathesis reaction with saturated aqueous $LiBF_4$ produced a free-flowing powder of mesityl(aryl)iodonium tetrafluoroborate as a regioisomer mixture (**6a, b**) with an overall yield of 12.7%. The subsequent ^{19}F-NMR analysis of cold fluorination reaction product revealed the mixture readily gives 3:2 ratio of tetra-Boc protected FIBG and tetra-Boc protected IFBG (**Supplemental Fig. 1B**).

Synthesis of ^{18}F-FIBG and ^{18}F-IFBG (8a, b)

We then attempted ^{18}F-labeling of **6** (step a in **Fig. 1C**). Although the procedure in the literature (*16*) provided the intermediate compound (**7a**, **b**), the RCY and reproducibility of the reaction were low (13.6 ± 10%, $n = 4$). By increasing the amount of $Cu(MeCN)_4OTf$ to five equivalents of the iodonium salt **6**, the highest RCY (63.9%) was obtained, yet with unsatisfying reproducibility (18.2 ± 19.7%, $n = 14$). In contrast, when we used an alternative Cu-catalyst ($Cu(OTf)_2$), a fair RCY was obtained with moderate reproducibility (19.7 ± 8.0%, $n = 13$). In the following deprotection reaction (**Fig. 1C**), we first tried to

replicate the previously developed procedure by directly adding 6N HCl to the reaction mixture and incubating it at 120°C (*15*). However, a large degree of defluorination and the formation of multiple by-products were observed, which decreased the recovery yield of **8** from **7** to less than 50%. By removing Cu and unreacted $^{18}F^-$, and by reducing the temperature to 70°C, ^{18}F-FIBG and ^{18}F-IFBG (**8a, b**) could be obtained in almost quantitative yield from **7a, b**. The regioisomer separation was achieved using a semi-preparative HPLC with high radiochemical purity (> 99%, **supplemental Figs 3**). The products **8a** and **8b** were obtained with an overall RCY of 5.06 ± 1.73% and 2.75 ± 0.95%, respectively (decay-corrected, *n* = 4).

In Vitro Profiles of Radiolabled MIBG Derivatives in PC-12 Cells

The accumulation of ^{18}F-FIBG in pheochromocytoma cells was approximately 1.5-fold higher than that of MIBG (**supplemental Fig. 4A**), whereas the accumulation of ^{18}F-IFBG was approximately 0.75-fold lower than that of MIBG. The uptake of all compounds was decreased by NET inhibitors to comparable levels (**supplemental Fig. 4B**). The uptake levels of ^{125}I-FIBG was also higher than that of MIBG in the 3D cell culture model, and a comparable release profile was found between FIBG and MIBG (**supplemental Fig. 5A and B, respectively**). As shown in **supplemental Fig. 5C**, FIBG exhibited greater cytotoxic effects at doses higher than 1 MBq/mL.

Biodistribution of ^{18}F-FIBG and ^{18}F-IFBG in Mice

We next evaluated the biodistribution profiles of ^{18}F-FIBG, ^{18}F-IFBG, and the regioisomer mixture in comparison with ^{125}I-MIBG (**Fig. 2**) in PC-12-bearing mice 1 h after injection. All fluorinated compounds showed the highest uptake within the tumor, which is similar to the distribution pattern of MIBG. Tumor uptake of ^{18}F-FIBG was slightly higher than that of ^{125}I-MIBG, although the difference was not statistically significant (41.5 ± 14.5 vs 35.4 ± 13.3%ID/g, respectively). In contrast, tumor uptake of ^{18}F-IFBG was approximately half that of ^{18}F-FIBG (18.6 ± 10.4%ID/g, $P < 0.05$). There was no significant difference between the tumor uptake of the regioisomer mixture and ^{125}I-MIBG. Comparable biodistribution profiles were found between ^{18}F-FIBG and ^{125}I-FIBG, or ^{18}F-IFBG and ^{125}I-IFBG (**supplemental Fig. 6**). The biodistribution profiles of ^{125}I-FIBG and ^{125}I-MIBG up to 7 days were shown in Supplemental Table 1. The calculated absorbed dose of the red marrow, the critical organ for ^{131}I-MIBG, was 8.70 μSv/MBq and 5.03 μSv/MBq for ^{131}I-FIBG and ^{131}I-MIBG, respectively. The effective dose equivalent was 125 μSv/MBq and 80.9 μSv/MBq for ^{131}I-FIBG and ^{131}I-MIBG, respectively

PET Imaging

To evaluate the tumor detectability of ^{18}F-FIBG and ^{18}F-IFBG, PET imaging was performed in PC-12-bearing mice (**Figs 3**). As early as 1 h after injection, ^{18}F-FIBG, ^{18}F-IFBG, and the regioisomer mixture clearly depicted even small tumors (4 mm, indicated by an orange arrow). The tumor-to-

background ratios of ^{18}F-FIBG, ^{18}F-IFBG, and the regioisomer mixture were 9.92 ± 3.43 (n = 12), 6.95 ± 1.42 (n = 6), and 18.4 (n = 1), respectively. In the 2 h image, ^{18}F-FIBG showed improved tumor-to-background ratios (13.3 ± 4.33, n = 12, $P < 0.05$, **supplemental Fig. 7**).

Tumor Retention of ^{125}I-FIBG and ^{131}I-MIBG in PC-12 Bearing Mice up to 5 days

The biodistribution profiles of ^{125}I-FIBG and ^{131}I-MIBG in PC-12-bearing mice up to 5 days post-injection are shown in **Supplemental Table 2**. Overall, FIBG showed a similar biodistribution profile to MIBG, although the initial uptake was higher than MIBG in almost all organs. A relatively fast clearance of FIBG from non-target organs (low NET-expressing) was noted. In contrast, in the NET-positive tissue such as the heart, adrenal glands, and tumor, FIBG was retained for longer and higher than MIBG for up to 5 days. In particular, FIBG accumulated in the tumor higher than it did in any other tissue during the entire observation period. The uptake peaked 24 h after injection (83.9 ± 7.37 %ID/g), with 18.4 ± 3.78 %ID/g remaining 5 days later. In contrast, the uptake of MIBG peaked 3 to 6 hours after injection, with little remaining 5 days later **(Fig. 4)**.

Tumor Growth Inhibition Effect of ^{131}I-FIBG

The tumor growth curves of PC-12 xenografts after administration of ^{131}I-FIBG or ^{131}I-MIBG are shown in **Fig. 5A**. At doses higher than 3 MBq, a single treatment with ^{131}I-FIBG suppressed the tumor

growth rate as compared to the saline-injected control group ($P < 0.0001$). Injections of 10 MBq of ^{131}I-MIBG resulted in a 2.5-fold increase in tumor volume ($T_{2.5}$) 22.6 ± 2.88 days after injection (**Supplemental Table 3**). The same dose of ^{131}I-FIBG resulted in $T_{2.5}$ for a longer period of time (31.7 ± 2.88 days, $P = 0.033$). Even at lower doses (3 MBq and 5 MBq), ^{131}I-FIBG administration delayed $T_{2.5}$ as compared to ^{131}I-MIBG (10 MBq), although this difference was not statically significant. No significant difference was observed in the body weight change (**Fig. 5B**).

Relationship between ^{18}F-FIBG Uptake and ^{18}F-FDGUptake or the Growth Inhibition Effect of ^{131}I-FIBG in PC-12 Tumors

Reflecting that xenograft tumors derived from PC-12 shows various differentiation states and uptake levels of MIBG derivatives (*18*) , the PC-12 tumor showed various SUV_{max} values in the pre-treatment ^{18}F-FIBG-PET image. In the linear regression analysis of pre-treatment PET imaging, ^{18}F-FIBG uptake and ^{18}F-FDG uptake showed a strong inverse correlation in the PC-12 xenograft tumor ($n = 9$, Pearson's correlation = -0.88, $P < 0.05$, **Fig. 6A**). Uptake of ^{18}F-FIBG also showed a strong inverse correlation with relative tumor volume of the PC-12 xenograft 33 days after the treatment of ^{131}I-FIBG ($n = 9$, Pearson's correlation = -0.76, $P < 0.05$, **Fig. 6B**). **Figs 6C and 6D** show representative PET images with high ^{18}F-FIBG uptake and low ^{18}F-FDG uptake, or low ^{18}F-FIBG uptake and high ^{18}F-FDG uptake, respectively. Additionally to the contrasting levels in these tumors, ^{18}F-FIBG and ^{18}F-FDG showed visibly

different intratumoral distribution. Change in tumor size between the two scans was negligible.

DISCUSSION

This study established a 2-step-radiofluorination method to produce ^{18}F-FIBG a promising diagnostic agent for NET-expressing tumors. In spite of the structural similarities, the additional iodine in ^{18}F-FIBG made it challenging to apply the radiofluorination methods used for the production of ^{18}F-MFBG (*13-15*). Indeed the additional iodine affected all precursor preparation, radiofluorination, and deprotection steps. First, among the various methods tested (*19-21*), the reaction developed by DiMagno et al. (*22*) was solely amenable to produce a single iodine substituted precursor **6**, because the ^{18}F-fluoride labile leaving groups are introduced via a substitution reaction with iodine. Secondly, 5 equivalent of $Cu(OTf)_2$ was required to produce radiofluorinated intermediate compound **7**, presumably due to the presence of multiple nitrogen atoms in the guanidine group and the additional iodine, both of which are also able to interact with Cu. Finally, in the next deprotection step, a moderate temperature (70°C) turned out to be effective in maintaining the recovery yield of **8** better than the initial harsh conditions by preventing temperature-dependent deiodination (*8*). The following HPLC regioisomer separation finally produced isomerically pure ^{18}F-FIBG (**8a**) and ^{18}F-IFBG (**8b**).

The subsequent in vitro and in vivo studies revealed the tumor imaging potential of the isolated ^{18}F-FIBG. At 1 h post-injection, ^{18}F-FIBG showed similar biodistribution profiles with ^{125}I-MIBG, which enabled clear visualization of the tumor in the PET imaging. Considering clinical situation, a 24 h uptake period is required for single-photon imaging of ^{123}I-MIBG, due to the slow clearance of ^{123}I-MIBG and

the resolution issue. The similarly high initial background uptake of ^{18}F-FIBG may also be problematic. However, as our 2 h PET image showed an improved tumor-to-background ratio due to clearance from non-target organs and persistent uptake within the tumor, the late phase image may improve the detectability of ^{18}F-FIBG. In addition, the advantage of PET probes over single-photon probes in terms of the detectability has been well documented elsewhere (*9*). The first-in-human trial of ^{18}F-MFBG indeed demonstrated that ^{18}F-MFBG can depict the tumor as early as 1 h after injection, despite its decreased tumor uptake versus *I-MIBG (*1*). It is worth investigating tumor imaging capability of ^{18}F-FIBG in more clinically relevant models with various NET expression levels in the further studies.

To evaluate if we could use the regioisomer mixture without needing cumbersome HPLC separation, we also compared the properties of ^{18}F-IFBG. Both in vitro and in vivo studies showed its reduced uptake in the PC-12 cells, though ^{18}F-IFBG and the regioisomer mixture also clearly depicted the PC-12 tumor in the PET imaging. The distribution patterns of ^{18}F-FIBG and ^{18}F-IFBG were comparable with their radioiodine-labeled counterparts, which indicates that their radioactivity represents biodistribution of the intact compounds. The NET-positive cells take up MIBG derivatives by either NET mediated specific uptake or passive diffusion (*23*). Because 1) all NET inhibitors reduced uptake of each probe to a similar extent and 2) FIBG and IFBG should have comparable lipophilicities, the difference in their uptake may be attributed to their affinity for NET. These results suggest that the positions of iodine and fluorine in the aromatic ring affect the affinity for NET, in addition to the lipophilicity of the

compound (*24*), and thus the regioisomer separation is recommended.

The high and prolonged uptake of FIBG within the tumor shown in the long-term in vivo biodistribution studies suggested the possibility of ^{131}I-FIBG to improve therapeutic efficacy by extending the effective half-life in the tumor, along with the long physical half-life of ^{131}I. Given that FIBG and MIBG showed comparable release profiles in vitro, various factors, such as re-uptake in the surrounding cells, lipophilicity, and deiodination tolerance of the compound, must have contributed differently in biological situation and caused prolonged retention of FIBG in the xenograft tumor.

As expected, ^{131}I-FIBG demonstrated a better therapeutic effect than ^{131}I-MIBG both in vitro and in vivo. The therapeutic efficacy of ^{131}I-MIBG is limited because myelosuppression restricts adequate tumoricidal dose administration to patients, though numerous clinical studies suggest a dose dependent response rate for ^{131}I-MIBG therapy (*25*). The absorbed radiation dose estimate of the red marrow showed approximately 1.7-fold higher values for ^{131}I-FIBG due to its relatively higher normal organ uptakes versus ^{131}I-MIBG, therefore maximum tolerated dose of ^{131}I-FIBG should be smaller than that of ^{131}I-MIBG. However, as ^{131}I-FIBG 3 MBq group showed comparable $T_{2.5}$ with that of ^{131}I-MIBG 10 MBq group, its high and prolonged tumor uptake would allow higher and more selective radiation dose exposure in the tumor. Further evaluation for the maximum tolerated dose and cumulative dose estimate in various tumor conditions are necessary to maximize the therapeutic efficacy of targeted-radiation therapy with ^{131}I-FIBG, and consolidate its usefulness in comparison with ^{131}I-MIBG.

The correlation between the SUV_{max} of ^{18}F-FIBG-PET and the therapeutic effect of ^{131}I-FIBG suggested the usefulness of pre-therapy ^{18}F-FIBG-PET for selecting patient suitable for ^{131}I-FIBG therapy, in addition to its potential capability of lesion detection and therapeutic monitoring. The radiation dose-estimation methods for ^{123}I-MIBG has not been established primarily due to the semi-quantitative nature and resolution issues, and the heterogeneous expression of NET at multiple sites (*25*). Although the applicability of the short-lived PET tracer like ^{18}F to estimate therapeutic absorbed doses requires further investigations, two retrospective studies exhibited the association of early lesion uptake and absorbed dose after PET scans with ^{68}Ga-labeled somatostatin analogs (*26,27*). To evaluate if the pre-therapy ^{18}F-FIBG uptake is associated with absorbed radiation dose of the tumor may be the objective of the future research.

Of note, our data confirmed the strong inverse correlation between uptake levels of an MIBG analog and ^{18}F-FDG, as several clinical studies observed differential uptake patterns of MIBG and ^{18}F-FDG (*3,28*). This is likely due to the individual microenvironmental differences of the implanted area, such as accessibility to a large blood vessel. The poorly differentiated tumor sites are known to either decrease MIBG in NET-expressing tumors or increase ^{18}F-FDG uptake in various types of cancer (*25,29,30*). These results suggest that ^{18}F-FIBG, together with ^{18}F-FDG, could be used to develop optimum combination therapy for ^{131}I-FIBG treatment (*4*) or therapeutic monitoring.

There are several limitations in our study. First, although we were able to simplify the radiolabeling method, the yield is still low and the procedures are rather complicated for clinical use,

especially as it requires regioisomer separation. Further studies are required to optimize the radiosynthetic procedure including selective synthesis of isomerically pure ^{18}F-FIBG and the development of an automated method. Secondly, the data need deliberate interpretation as we used only one xenograft model with exceptionally high NET expression levels, whereas clinical NET-expressing tumors express heterogeneous phenotypes. Nevertheless, the promising properties shown in this study suggested FIBG warrant further evaluation in more clinically relevant models such as various neuroblastoma xenografts and their metastatic models.

In conclusion, we found that Cu-mediated radiofluorination successfully produces ^{18}F-FIBG in two steps plus HPLC purification. Excellent tumor detectability and uptake comparable with MIBG was proven with ^{18}F-FIBG. Moreover, ^{131}I-FIBG showed a greater therapeutic effect in malignant pheochromocytomas than ^{131}I-MIBG. These results support the potential usefulness of FIBG as a diagnostic as well as a therapeutic agent for the management of NET-expressing tumors.

DISCLOSURE

This work is supported by JSPS KAKENHI Grant 26860981 for A. Yamaguchi. The authors declare no other potential conflicts of interest.

ACKNOWLEDGEMENTS

We are grateful to N. Ichiishi (Department of Chemistry, University of Michigan) and P. J. H. Scott (Department of Radiology and Interdepartmental Program in Medicinal Chemistry, University of Michigan) for providing expert technical advice regarding ^{18}F-labeling, and also to T. Ogasawara (Cyclotoron facility, Gunma University Hospital) for the production of ^{18}F-fluoride and ^{18}F-FDG.

REFERENCES

1. Pandit-Taskar N, Modak S. Norepinephrine transporter as a target for imaging and therapy. *J Nucl Med.* 2017;58:39S-53S.

2. Kayano D, Kinuya S. Iodine-131 metaiodobenzylguanidine therapy for neuroblastoma: reports so far and future perspective. *ScientificWorldJournal.* 2015;2015:189135.

3. Sharp SE, Shulkin BL, Gelfand MJ, Salisbury S, Furman WL. 123I-MIBG scintigraphy and 18F-FDG PET in neuroblastoma. *J Nucl Med.* 2009;50:1237-1243.

4. Matthay KK, George RE, Yu AL. Promising therapeutic targets in neuroblastoma. *Clin Cancer Res.* 2012;18:2740-2753.

5. Vaidyanathan G, McDougald D, Koumarianou E, Choi J, Hens M, Zalutsky MR. Synthesis and evaluation of 4-[^{18}F]fluoropropoxy-3-iodobenzylguanidine ([^{18}F]FPOIBG): A novel ^{18}F-labeled analogue of MIBG. *Nuclear Medicine and Biology.* 2015;42:673-684.

6. Zhang H, Huang R, Cheung NK, et al. Imaging the norepinephrine transporter in neuroblastoma:

a comparison of [^{18}F]-MFBG and ^{123}I-MIBG. *Clin Cancer Res.* 2014;20:2182-2191.

7. Gaertner FC, Wiedemann T, Yousefi BH, et al. Preclinical evaluation of 18F-LMI1195 for in vivo imaging of pheochromocytoma in the MENX tumor model. *J Nucl Med.* 2013;54:2111-2117.

8. Vaidyanathan G, Affleck DJ, Zalutsky MR. (4-[^{18}F]fluoro-3-iodobenzyl)guanidine, a potential MIBG analogue for positron emission tomography. *J Med Chem.* 1994;37:3655-3662.

9. Baum RP, Kulkarni HR, Carreras C. Peptides and receptors in image-guided therapy: theranostics for neuroendocrine neoplasms. *Semin Nucl Med.* 2012;42:190-207.

10. Vaidyanathan G, Affleck DJ, Zalutsky MR. Validation of 4-[fluorine-18]fluoro-3-iodobenzylguanidine as a positron-emitting analog of MIBG. *J Nucl Med.* 1995;36:644-650.

11. Vaidyanathan G, Zhao XG, Strickland DK, Zalutsky MR. No-carrier-added iodine-131-FIBG: evaluation of an MIBG analog. *J Nucl Med.* 1997;38:330-334.

12. Preshlock S, Tredwell M, Gouverneur V. 18F-Labeling of arenes and heteroarenes for

applications in positron emission tomography. *Chemical Reviews.* 2016;116:719-766.

13. Rotstein BH, Wang L, Liu RY, et al. Mechanistic studies and radiofluorination of structurally diverse pharmaceuticals with spirocyclic iodonium(III) ylides. *Chem Sci.* 2016;7:4407-4417.

14. Preshlock S, Calderwood S, Verhoog S, et al. Enhanced copper-mediated ^{18}F-fluorination of aryl boronic esters provides eight radiotracers for PET applications. *Chemical Communications.* 2016;52:8361-8364.

15. Hu B, Vāvere AL, Neumann KD, Shulkin BL, DiMagno SG, Snyder SE. A practical, automated synthesis of meta-[^{18}F]fluorobenzylguanidine for clinical use. *ACS Chemical Neuroscience.* 2015;6:1870-1879.

16. Ichiishi N, Brooks AF, Topczewski JJ, Rodnick ME, Sanford MS, Scott PJH. Copper-catalyzed [^{18}F]fluorination of (mesityl)(aryl)iodonium salts. *Organic Letters.* 2014;16:3224-3227.

17. Vaidyanathan G, Affleck DJ, Alston KL, Zalutsky MR. A tin precursor for the synthesis of no-carrier-added [*I]MIBG and [^{211}At]MABG. *Journal of Labelled Compounds and Radiopharmaceuticals.*

2007;50:177-182.

18. Watanabe S, Hanaoka H, Liang JX, Iida Y, Endo K, Ishioka NS. PET imaging of norepinephrine transporter-expressing tumors using ^{76}Br-meta-bromobenzylguanidine. *J Nucl Med.* 2010;51:1472-1479.

19. Mossine AV, Brooks AF, Makaravage KJ, et al. Synthesis of [^{18}F]arenes via the copper-mediated [^{18}F]fluorination of boronic acids. *Organic Letters.* 2015;17:5780-5783.

20. Tredwell M, Preshlock SM, Taylor NJ, et al. A general copper-mediated nucleophilic ^{18}F fluorination of arenes. *Angew Chem Int Ed Engl.* 2014;53:7751-7755.

21. Qiu D, Mo F, Zheng Z, Zhang Y, Wang J. Gold(III)-catalyzed halogenation of aromatic boronates with N-halosuccinimides. *Org Lett.* 2010;12:5474-5477.

22. Qin L, Hu B, Neumann KD, et al. A mild and general one-pot synthesis of densely functionalized diaryliodonium salts. *European J Org Chem.* 2015;2015:5919-5924.

23. Jaques S, Jr., Tobes MC, Sisson JC. Sodium dependency of uptake of norepinephrine and m-

iodobenzylguanidine into cultured human pheochromocytoma cells: evidence for uptake-one. *Cancer Res.* 1987;47:3920-3928.

24. Vaidyanathan G, Shankar S, Affleck DJ, Welsh PC, Slade SK, Zalutsky MR. Biological evaluation of ring- and side-chain-substituted m-iodobenzylguanidine analogues. *Bioconjug Chem.* 2001;12:798-806.

25. Grunwald F, Ezziddin S. 131I-metaiodobenzylguanidine therapy of neuroblastoma and other neuroendocrine tumors. *Semin Nucl Med.* 2010;40:153-163.

26. Hanscheid H, Sweeney RA, Flentje M, et al. PET SUV correlates with radionuclide uptake in peptide receptor therapy in meningioma. *Eur J Nucl Med Mol Imaging.* 2012;39:1284-1288.

27. Ezziddin S, Lohmar J, Yong-Hing CJ, et al. Does the pretherapeutic tumor SUV in 68Ga DOTATOC PET predict the absorbed dose of 177Lu octreotate? *Clin Nucl Med.* 2012;37:e141-147.

28. Melzer HI, Coppenrath E, Schmid I, et al. ^{123}I-MIBG scintigraphy/SPECT versus ^{18}F-FDG PET in paediatric neuroblastoma. *Eur J Nucl Med Mol Imaging.* 2011;38:1648-1658.

29. Vesselle H, Salskov A, Turcotte E, et al. Relationship between non-small cell lung cancer FDG uptake at PET, tumor histology, and Ki-67 proliferation index. *J Thorac Oncol.* 2008;3:971-978.

30. Seo S, Hatano E, Higashi T, et al. Fluorine-18 fluorodeoxyglucose positron emission tomography predicts tumor differentiation, P-glycoprotein expression, and outcome after resection in hepatocellular carcinoma. *Clin Cancer Res.* 2007;13:427-433.

FIGURE 1.

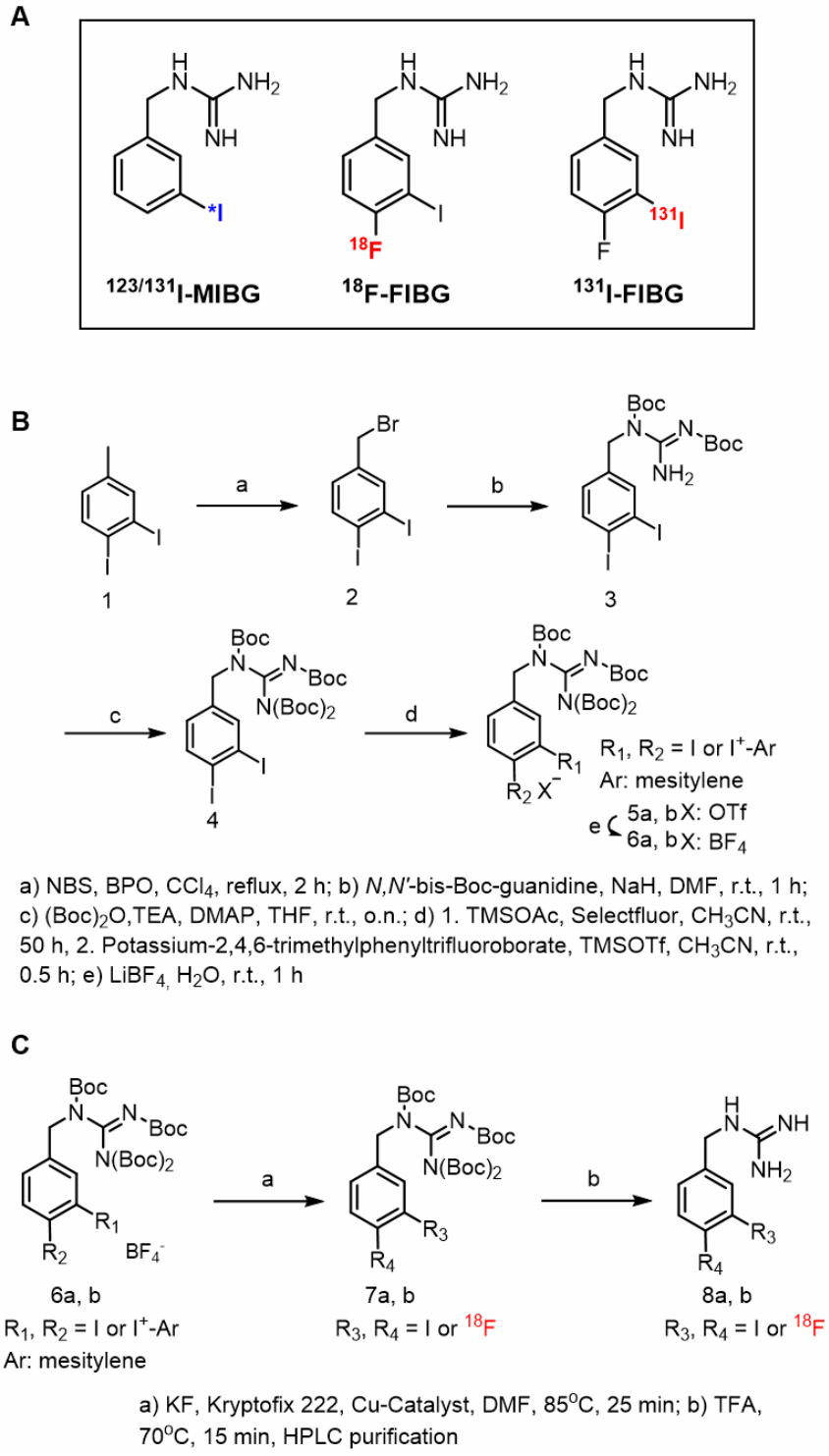

FIGURE 1. A, chemical structures of MIBG and FIBG. B, synthesis of **6a, b**. C, radiosynthesis of **8a, b**.

FIGURE 2.

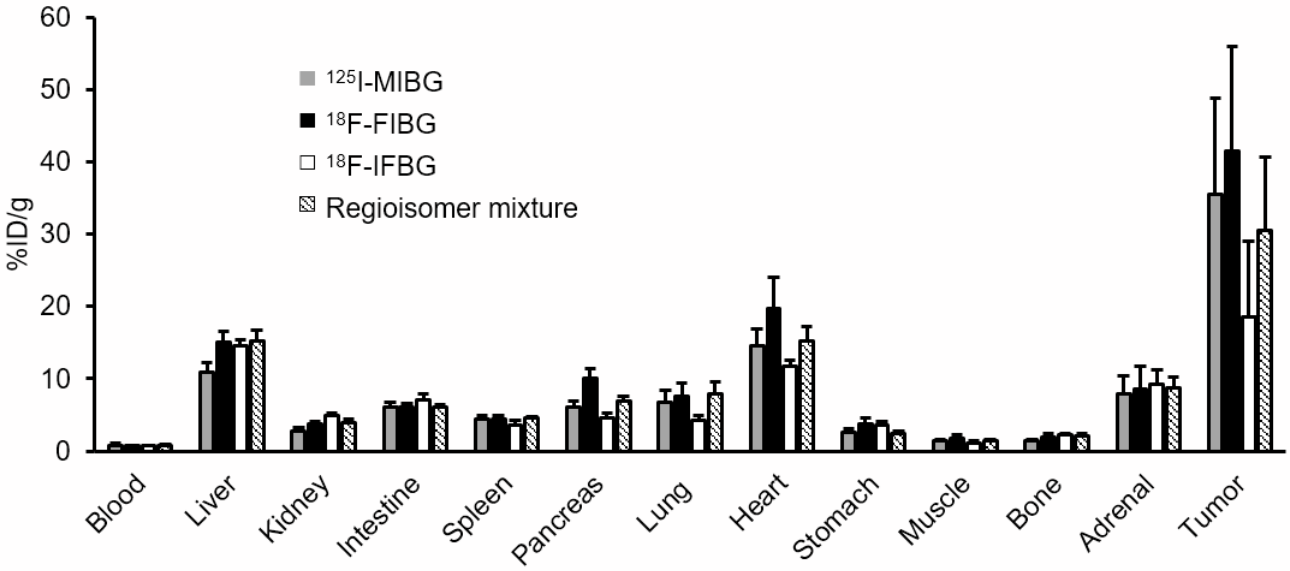

FIGURE 2. Biodistribution profiles of $^{18}F/^{125}I$-MIBG derivatives in PC-12-bearing mice at 1 h after injection (mean ± SD; 4-5 per group).

FIGURE 3.

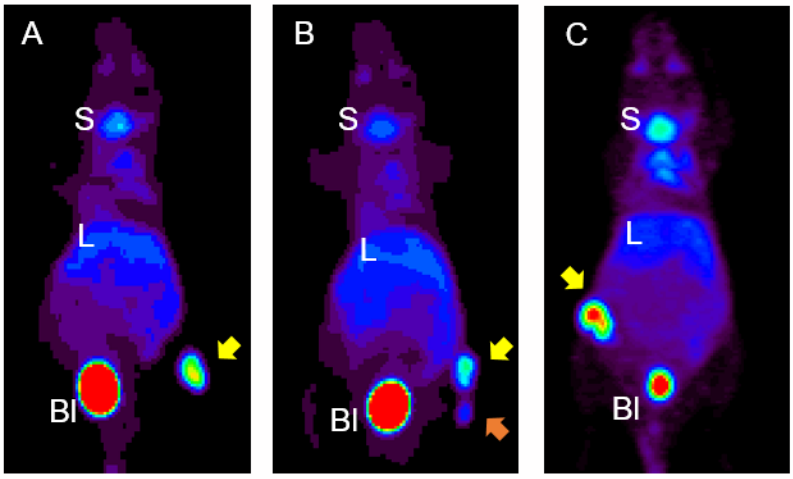

FIGURE 3. Representative PET images with ^{18}F-FIBG (A), ^{18}F-IFBG (B), and the regioisomer mixture (C) in PC-12-bearing mice at 1 h after injection. Arrows indicate tumor locations. S: Salivary gland, L: Liver, Bl: Bladder.

FIGURE 4.

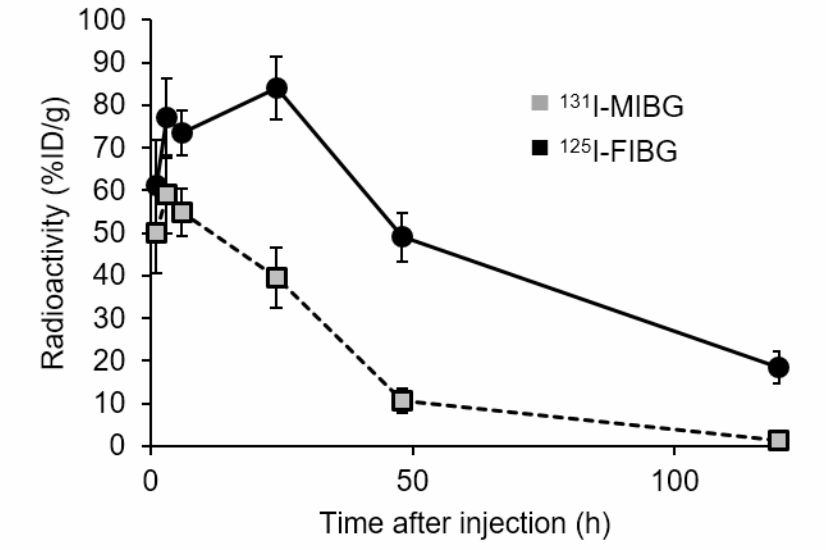

FIGURE 4. Tumor uptake of ^{125}I-FIBG and ^{131}I-MIBG in PC-12-bearing mice (Mean ± SD; 3-5 per group).

FIGURE 5.

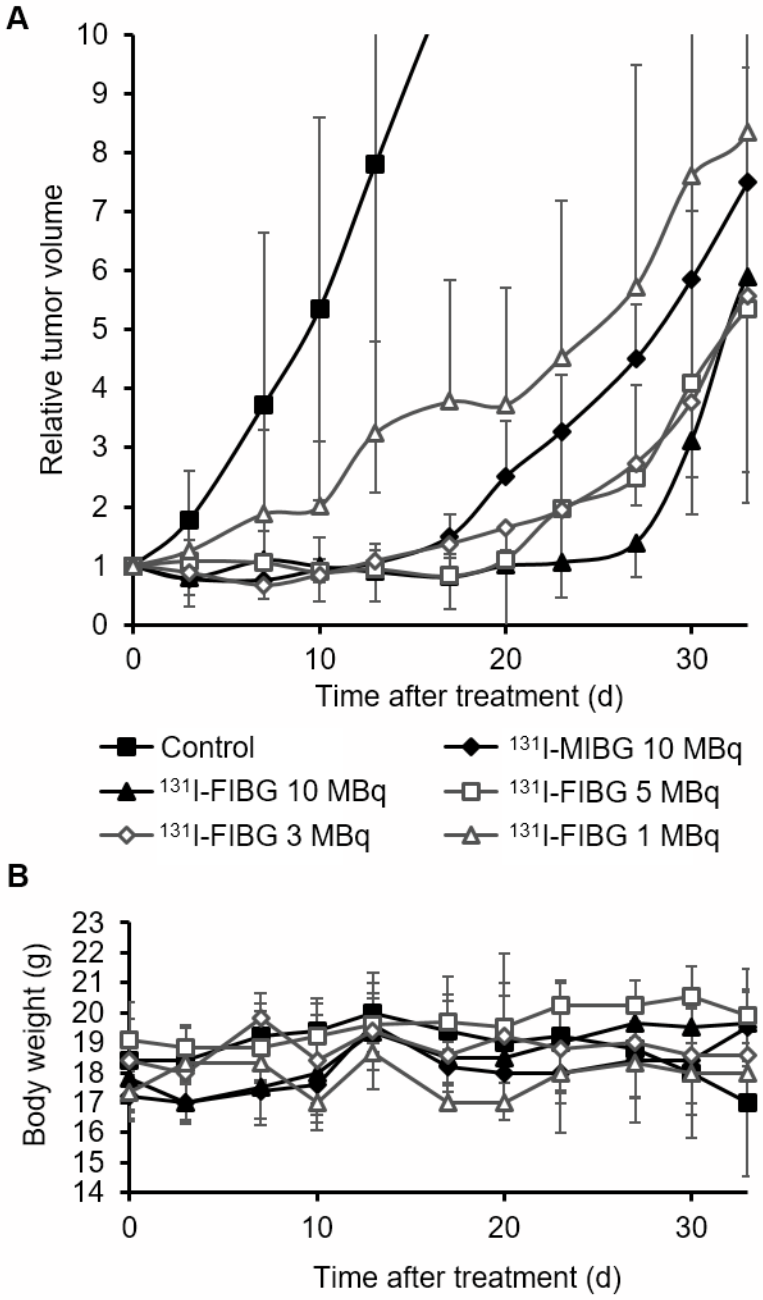

FIGURE 5. A, effect of ^{131}I-FIBG/MIBG on the growth of PC-12 tumor-bearing mice. B, body weight changes. Mean ± SD (at least n = 5 per group, except FIBG 1 MBq group (n = 3))

FIGURE 6.

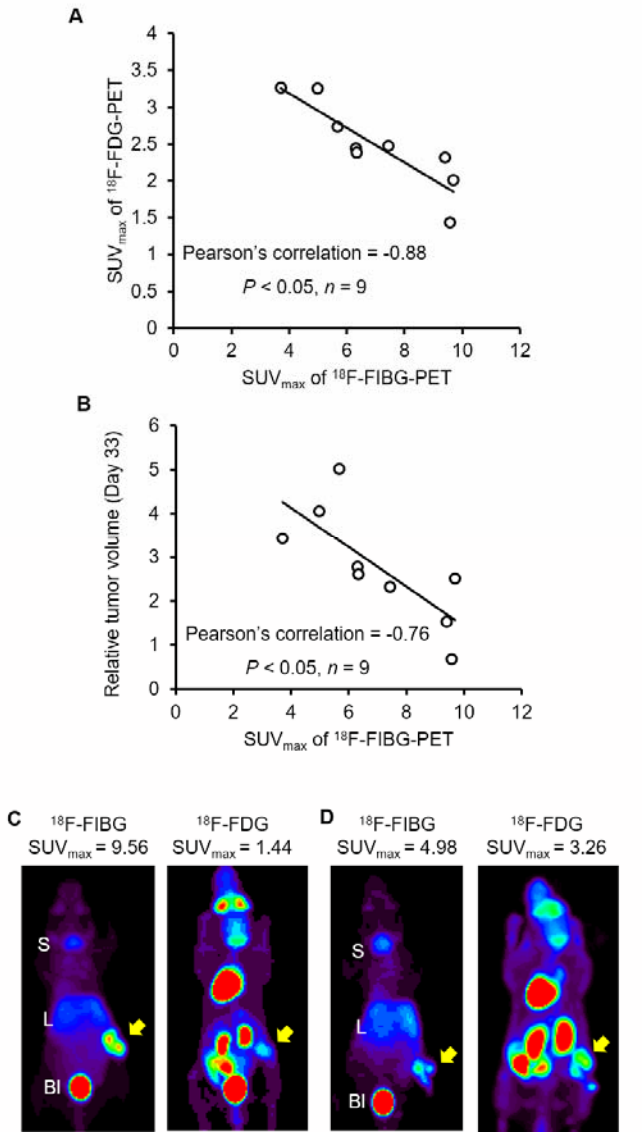

FIGURE 6. Relationship between ^{18}F-FIBG uptake and ^{18}F-FDG uptake (A), or relative tumor volume at day 33 after 5 MBq of ^{131}I-FIBG administration (B). The Pearson's correlation coefficient and *P* value are indicated (*n* = 9). C and D, representative pre-treatment ^{18}F-FIBG (left) and ^{18}F-FDG (right) PET image. Mouse with high (C) or low (D) ^{18}F-FIBG uptake. Yellow arrow indicates tumor location. S: Salivary gland, L: Liver, Bl: Bladder.

Supplementary data for FIBG for detection and therapy of NET expressing tumor

Supplementary Figures

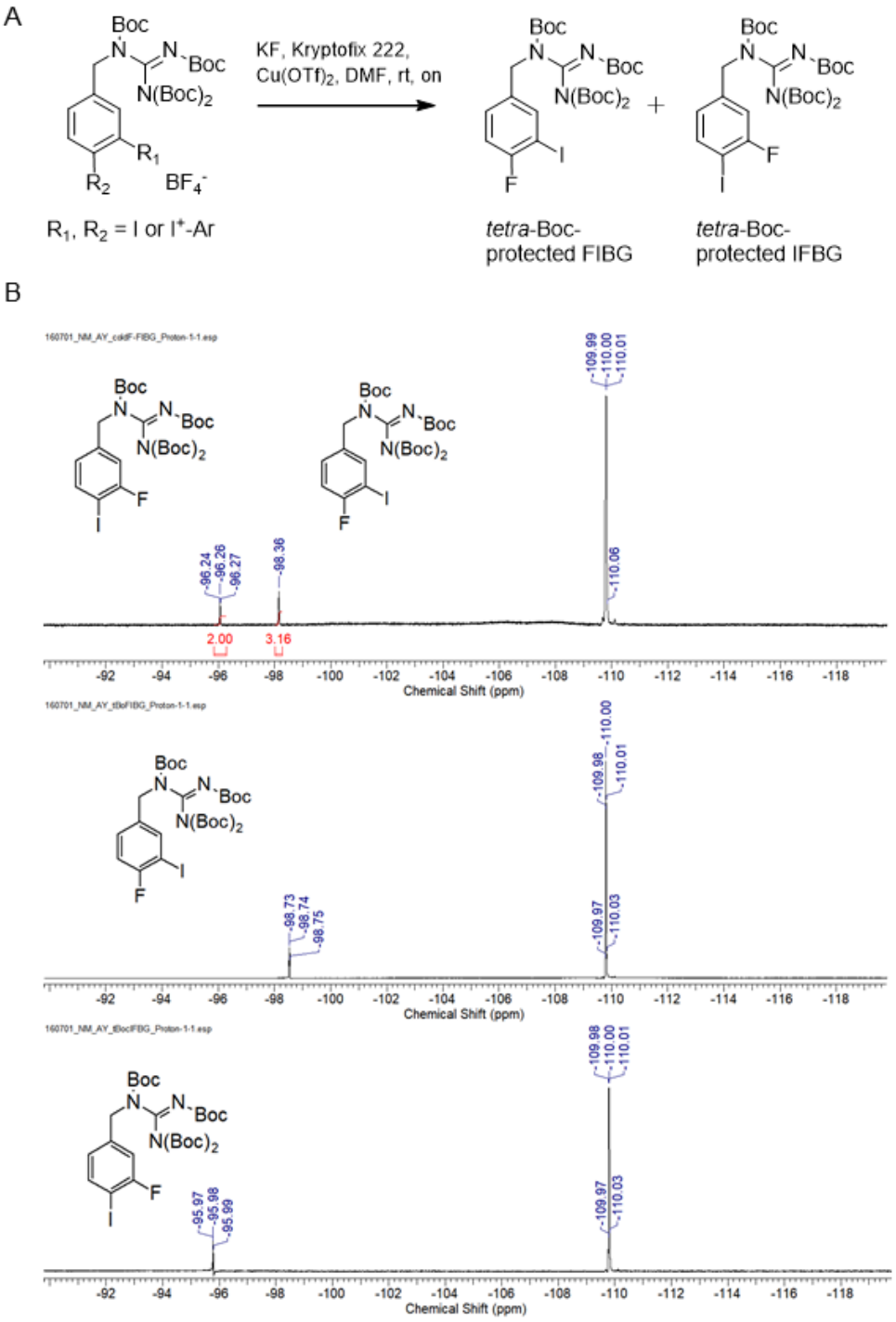

Supplemental Figure 1. Scheme and ^{19}F-NMR data for cold-^{19}F-fluorination. A, schematic image of the cold-^{19}F-fluorination reaction. B, ^{19}F-NMR spectrum (600 MHz, $CDCl_3$) of the resioisomer mixture in the cold-fluorination reaction (upper panel), isomerically pure *tetra*-Boc-protected FIBG (middle panel), and IFBG (lower panel). ^{19}F-NMR spectra are referenced based on the internal standard 1,3,5-trifluorobenzene (δ –110.00 ppm).

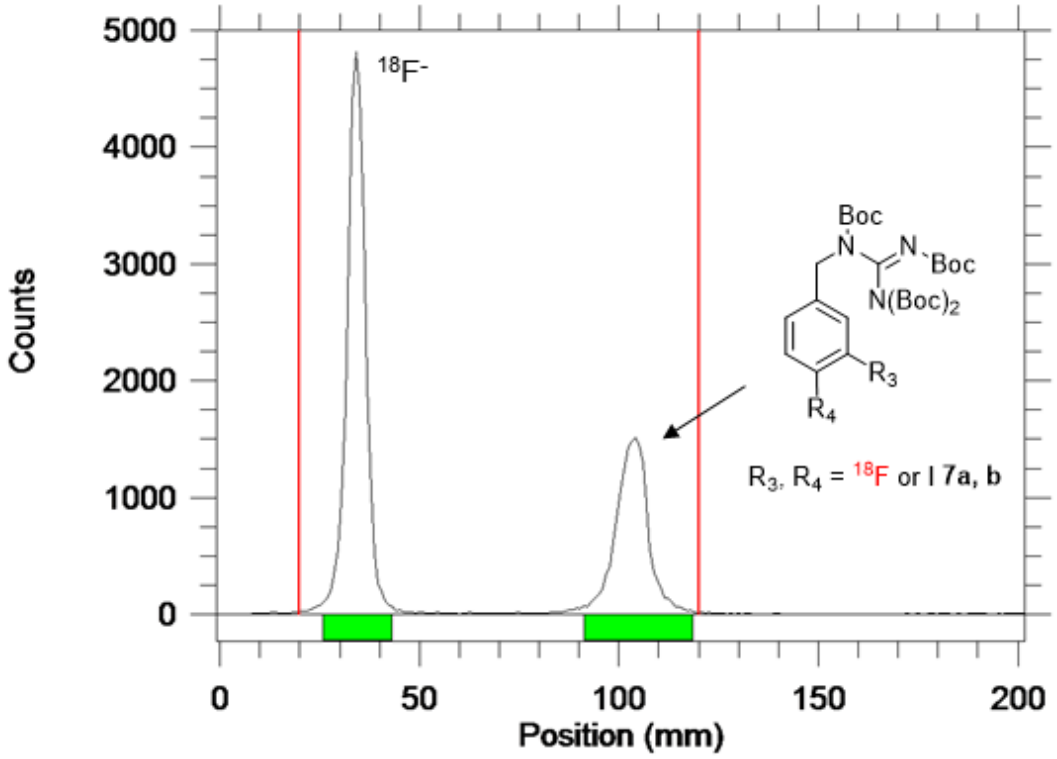

Supplemental Figure 2. Representative Radio-TLC results of the intermediate compound (**7a, b**). Eluent: hexane:ethyl acetate=1:1, Rf = 0.16: unreacted $^{18}F^-$, Rf = 0.8: **7a, b**

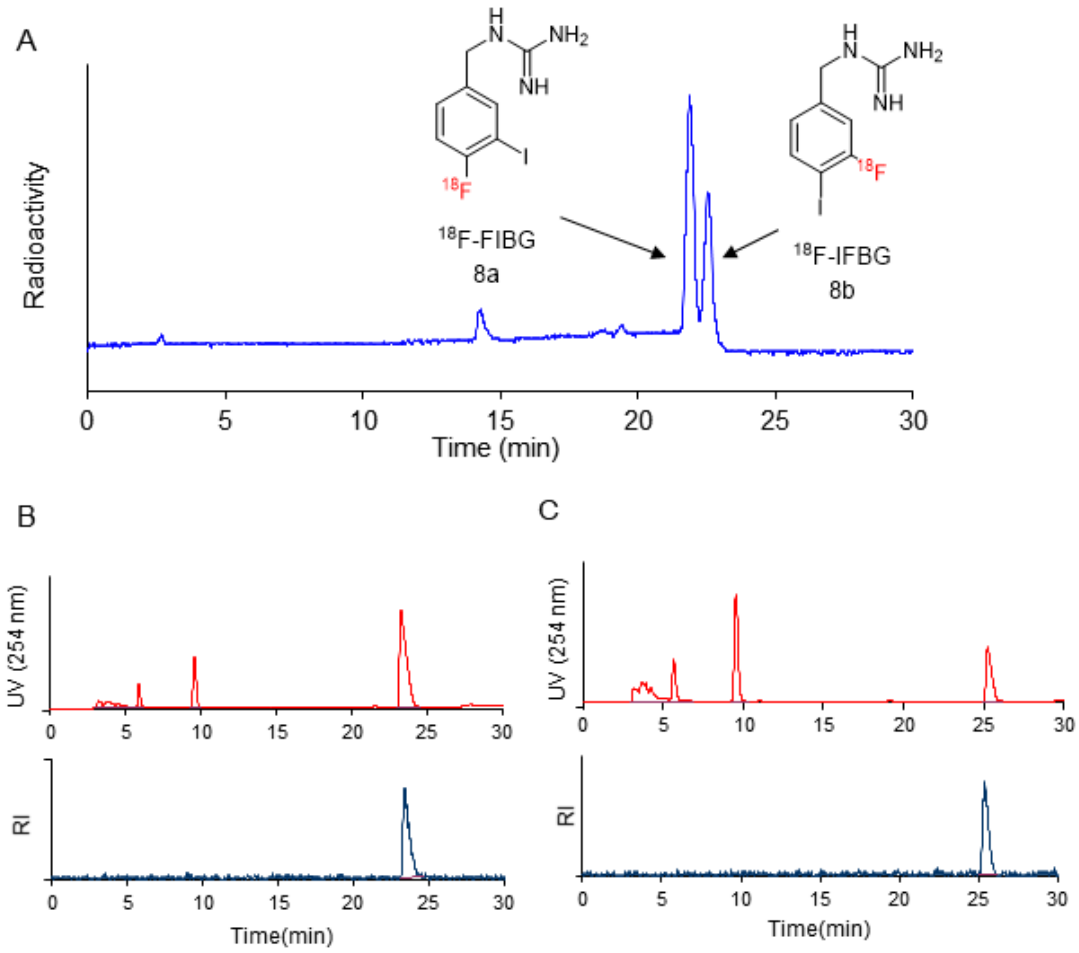

Supplemental Figure 3. HPLC profiles of ^{18}F-FIBG and ^{18}F-IFBG. A, semi-preparative HPLC. B and C, after purification spiked with cold standards. ^{18}F-FIBG (8a) with FIBG (B), ^{18}F-IFBG (8b) with IFBG (C). Semipreparative HPLC conditions: column COSMOSIL Cholester 10 mm I.D. × 250 mm; 5 μm (Nacalai Tesque); flow rate 5 mL/min; eluents A = 0.1% TFA (v/v) in water and B = 0.1% TFA (v/v) in methanol; Gradient 0-30 min, 25-45% B; 30-35 min, 45-100% B; detection UV-vis 254 nm, RI (γ detector). Analytical HPLC were performed by using a COSMOSIL Cholester column of 4 mm I.D. × 250 mm, at a flow rate of 1 mL/min. Another conditions were the same with those of semipreparative HPLC.

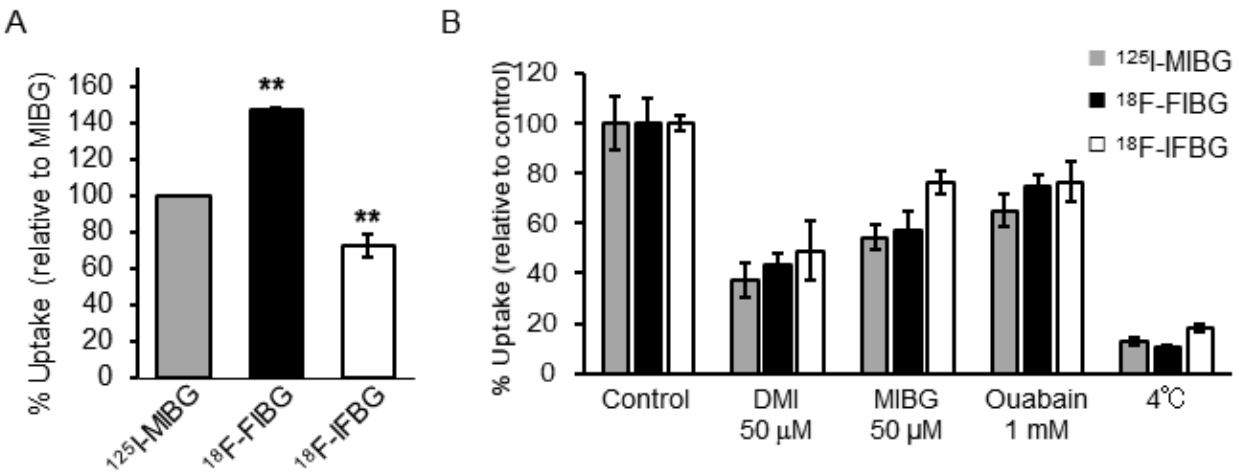

Supplemental Figure 4. A, relative uptake of ^{18}F-FIBG or ^{18}F-IFBG in PC-12 cells (n = 4; **, P < 0.01, paired t-test). B, effect of inhibitors on the uptake of MIBG analogs in PC-12 cells (mean ± SD; n = 4).

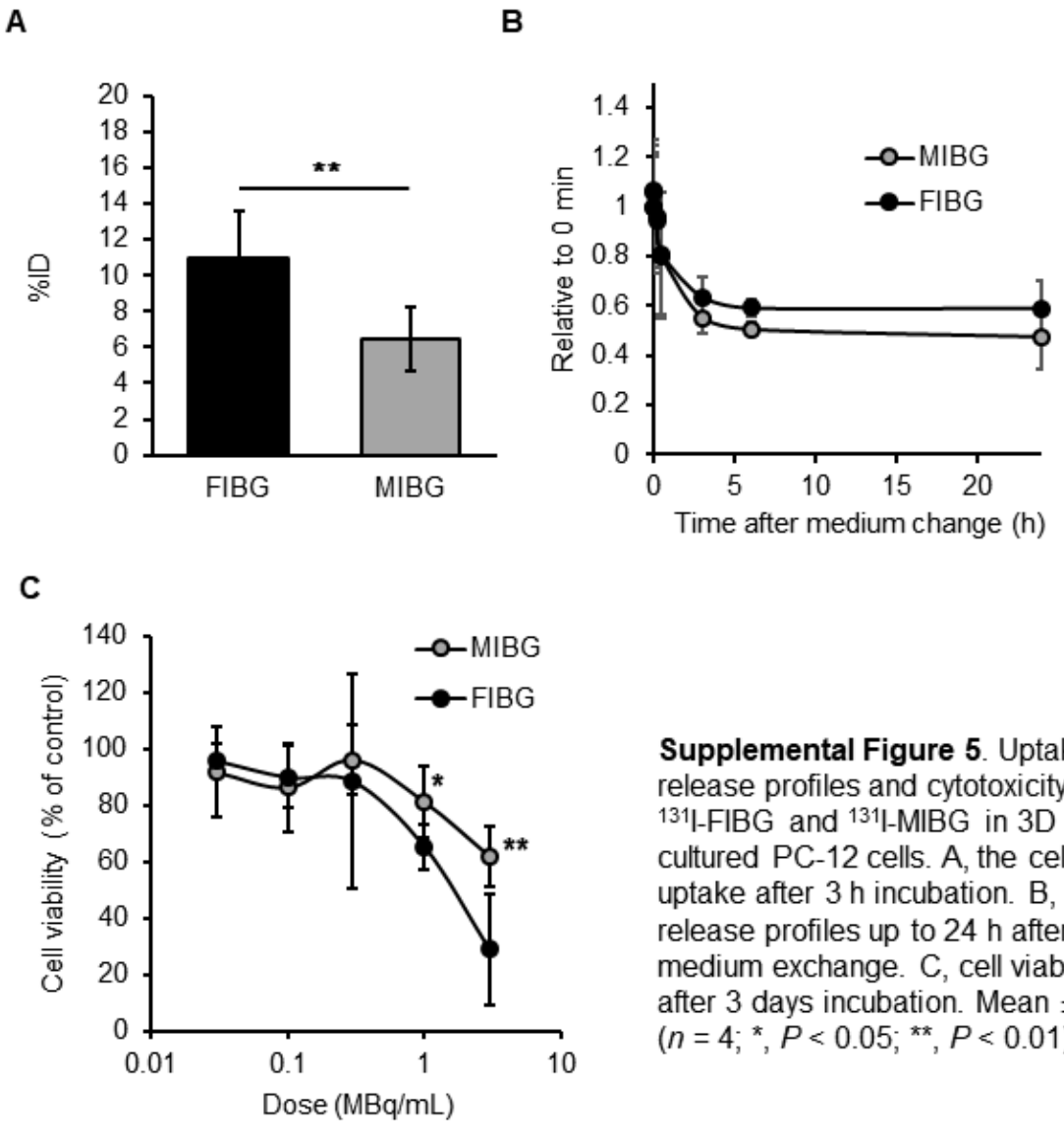

Supplemental Figure 5. Uptake, release profiles and cytotoxicity of ^{131}I-FIBG and ^{131}I-MIBG in 3D cultured PC-12 cells. A, the cellular uptake after 3 h incubation. B, release profiles up to 24 h after medium exchange. C, cell viability after 3 days incubation. Mean ± SD (n = 4; *, P < 0.05; **, P < 0.01)

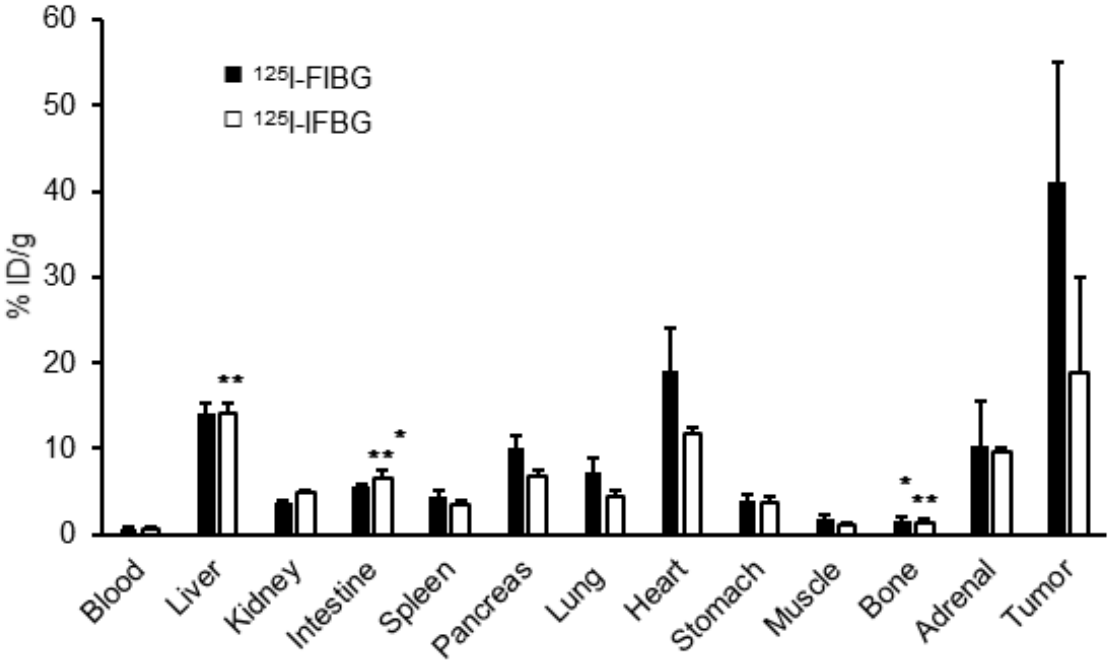

Supplemental Figure 6. Biodistribution profiles of ^{125}I-FIBG and ^{125}I-IFBG in PC-12 xenograft mice at 1 h after injection. Mean ± SD (n = 5 per group; *, $P < 0.05$; **, $P < 0.01$, data are compared with each ^{18}F-labeled counterpart by paired t-test)

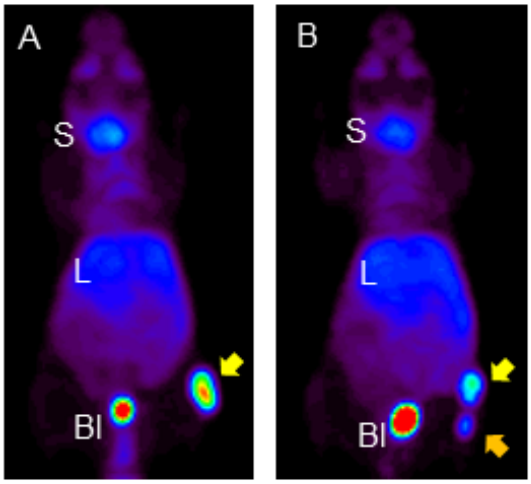

Supplemental Figure 7. Representative 2 h PET images of ^{18}F-FIBG and -^{18}F-IFBG in PC-12 xenograft. ^{18}F-FIBG (A) and ^{18}F-IFBG (B). Arrows indicate tumor locations. S: Salivary gland, L: Liver, Bl: Bladder.

Supplemental Table 1. Biodistribution profiles of ^{125}I-FIBG and ^{125}I-MIBG in normal mice.

%ID/g	^{125}I-FIBG							^{125}I-MIBG						
Time	10 m	1 h	3 h	6 h	1 day	3 days	7 days	10 m	1 h	3 h	6 h	1 day	3 days	7 days
Blood	0.81*	0.49	0.35	0.33	0.09	0.02	0.01	0.98	0.56	0.30	0.28	0.07	0.01	0.00
	0.09	0.11	0.10	0.09	0.02	0.01	0.00	0.13	0.11	0.05	0.03	0.01	0.01	0.00
Liver	7.33	8.89*	6.33*	4.69*	1.28*	0.46*	0.08*	6.62	7.19	2.98	2.35	0.48	0.09	0.03
	0.91	0.71	0.82	0.74	0.28	0.11	0.02	0.78	0.66	0.50	0.45	0.07	0.02	0.01
Kidney	7.40	2.29	1.34	1.38	0.51*	0.25	0.04	4.73	2.76	1.18	1.57	0.16	0.07	0.01
	2.33	0.32	0.30	0.13	0.11	0.11	0.03	0.72	0.55	0.22	1.19	0.07	0.02	0.01
Intestine	3.25	2.95	3.21	2.37	1.13*	0.41*	0.06*	3.97	3.63	2.43	2.74	0.65	0.11	0.02
	0.77	0.32	0.48	0.31	0.29	0.11	0.03	0.25	0.71	0.47	0.24	0.11	0.02	0.01
Spleen	3.85	2.36	1.78	2.03	1.38*	0.77*	0.06	3.52	2.13	1.50	1.55	0.31	0.04	0.01
	0.68	0.61	0.24	0.29	0.33	0.21	0.03	0.24	0.20	0.40	0.59	0.23	0.02	0.01
Pancreas	11.0*	6.74	3.90	3.95	1.19	0.43*	0.05*	9.29	6.53	2.69	2.19	0.41	0.07	0.00
	1.39	0.40	1.30	0.53	0.52	0.12	0.03	0.98	0.90	0.48	0.37	0.03	0.01	0.01
Lung	14.3	6.04	3.53	2.70	1.27*	0.35*	0.05	12.6	4.81	2.90	2.42	0.43	0.06	0.03
	1.24	1.27	0.52	0.16	0.20	0.09	0.03	3.06	0.33	0.50	0.32	0.16	0.01	0.03
Heart	11.5	10.4	9.62*	8.71*	6.09*	1.99*	0.23*	13.12	9.47	6.08	5.51	1.07	0.13	0.02
	1.01	1.58	1.33	1.29*	1.12	0.34	0.13	1.98	0.47	0.76	1.05	0.20	0.05	0.01
Stomach	2.32	2.11	1.18	1.22	0.57	0.27*	0.08	2.38	2.18	1.22	1.88	0.52	0.18	0.06
	0.73	0.16	0.39	0.25	0.12	0.02	0.05	0.57	0.67	0.25	0.24	0.03	0.04	0.01
Muscle	1.73	1.32	1.10	1.00	0.39*	0.15*	0.09	1.52	1.50	0.87	0.92	0.16	0.03	0.00
	0.57	0.17	0.37	0.25	0.13	0.05	0.16	0.56	0.34	0.18	0.15	0.05	0.02	0.00
Bone	1.92	1.49	1.76*	1.41	0.54	0.10	0.01	2.13	1.82	1.13	1.16	0.24	0.05	0.00
	0.20	0.59	0.16	0.43	0.22	0.05	0.01	0.64	0.25	0.22	0.46	0.08	0.04	0.01
Adrenal	12.9	11.3	11.3	9.37	17.4*	16.4*	10.2	12.7	9.24	5.92	15.2	13.3	8.46	7.39
	3.37	4.83	2.87	4.79	2.87	3.52	3.51	5.07	6.53	4.02	4.50	1.46	3.19	1.55

Data represent %ID/g (upper row: averaged, lower row: SD). ***** statistically significant ($P < 0.05$).

Supplemental Table 2. Biodistribution profiles of ^{131}I-FIBG and ^{125}I-MIBG in PC-12 tumor-bearing mice.

	FIBG						MIBG					
	1 h	3 h	6 h	24 h	48 h	5 days	1 h	3 h	6 h	24 h	48 h	5 days
Blood	1.50	0.94 †	0.55	0.13	0.07 †	0.03 †	2.51	1.01	0.70	0.10	0.08	0.02
	0.36	0.08	0.06	0.03	0.03	0.00	1.17	0.11	0.07	0.02	0.06	0.02
Liver	15.8	12.2	7.96	2.24	1.51	0.45	10.0	5.67	3.32	0.52	0.24	0.04
	2.26	0.11	0.58	0.22	0.28	0.04	1.48	0.25	0.39	0.07	0.03	0.01
Kidney	4.16	2.61	2.45	1.01	0.58	0.20	3.31	1.75	1.49	0.28	0.13	0.05
	0.25	0.17	0.25	0.11	0.13	0.03	0.41	0.20	0.25	0.05	0.02	0.02
Intestine	7.42	6.75 †	6.10	2.18	1.55	0.45	6.65	6.94	5.63	1.06	0.45	0.09
	0.94	0.41	0.61	0.17	0.37	0.05	0.86	0.50	0.65	0.06	0.10	0.03
Spleen	5.79	5.57	4.68	4.07	2.39	0.91	4.42	4.10	2.79	1.30	0.44	0.10
	0.40	0.46	0.48	0.36	0.73	0.16	0.62	0.26	0.17	0.18	0.18	0.04
Pancreas	10.2	7.83	6.92	2.40	1.45	0.32	6.80	3.87	2.63	0.54	0.18	0.01
	1.14	0.68	0.81	0.39	0.36	0.09	0.89	0.38	0.42	0.13	0.04	0.01
Lung	11.6	6.92	6.44	2.02	1.11	0.33	6.71	3.47	3.01	0.48	0.18	0.07
	1.94	2.15	0.75	0.17	0.25	0.03	1.02	0.85	0.62	0.09	0.07	0.02
Heart	18.9	16.81	17.55	9.87	5.19	1.25	13.2	9.40	7.58	1.79	0.56	0.10
	2.73	2.09	0.93	1.10	1.36	0.46	2.82	1.18	0.52	0.34	0.14	0.02
Stomach	6.94	5.74	4.35	1.63 †	1.38	0.77	11.0	8.44	5.26	1.07	0.68	0.24
	0.78	0.74	0.42	0.67	0.51	0.15	2.20	2.75	0.38	0.42	0.27	0.07
Muscle	1.57	1.31	1.02	0.47	0.26	0.03 †	1.22	0.80	0.78	0.20	0.08	0.02
	0.29	0.41	0.10	0.11	0.18	0.05	0.27	0.23	0.26	0.05	0.06	0.03
Adrenal	11.8	8.52 †	9.38 †	9.47	9.06	5.87	8.96	6.84	7.90	5.71	5.13	1.86
	3.73	3.47	2.22	2.32	3.17	0.65	4.04	1.65	2.48	1.10	1.70	2.13
Tumor	61.2	77.0	73.4	83.9	49.0	18.4	50.1	59.0	54.9	39.6	10.7	1.46
	10.6	9.38	5.30	7.37	5.67	3.78	9.38	9.18	5.62	7.14	2.76	0.36

Data represent %ID/g (upper row: averaged, lower row: SD). † statistically **not** significant by paired t-test ($P > 0.05$).

Supplementary Table 3. Days required for a 2.5-fold increase in volume of PC-12 tumor

Treatment	Days	*P*-value	
	Average (SD)	vs. control	vs. MIBG
Control	8.00 (3.08)		
MIBG 10 MBq	22.6 (2.88)	0.0003	
FIBG 10 MBq	31.7 (2.88)	< 0.0001	0.033
FIBG 5 MBq	29.8 (3.89)	< 0.0001	n.s.
FIBG 3 MBq	28.8 (5.22)	< 0.0001	n.s.
FIBG 1 MBq	15.7 (10.3)	n.s.	n.s.